Progress In Electromagnetics Research, PIER 32, 383–411, 2001

IMPLEMENTING THE PERFECTLY MATCHED LAYER ABSORBING BOUNDARY CONDITION WITH MIMETIC DIFFERENCING SCHEMES

M. W. Buksas

Los Alamos National Laboratory, MS B-258
Los Alamos, New Mexico 87545, USA

Abstract—This paper concerns the implementation of the perfectly matched layer (PML) absorbing boundary condition in the framework of a mimetic differencing scheme for Maxwell's Equations.

We use mimetic versions of the discrete curl operator on irregular logically rectangular grids to implement anisotropic tensor formulation of the PML. The form of the tensor we use is fixed with respect to the grid and is known to be perfectly matched in the continuous limit for orthogonal coordinate systems in which the metric is constant, i.e. Cartesian coordinates, and quasi-perfectly matched (quasi-PML) for curvilinear coordinates. Examples illustrating the effectiveness and long-term stability of the methods are presented. These examples demonstrate that the grid-based coordinate implementation of the PML is effective on Cartesian grids, but generates systematic reflections on grids which are orthogonal but non-Cartesian (quasi-PML). On non-orthogonal grids progressively worse performance of the PML is demonstrated.

The paper begins with a summary derivation of the anisotropic formulation of the perfectly matched layer and mimetic differencing schemes for irregular logically rectangular grids.

1. BACKGROUND

1.1. The PML Absorbing Boundary Condition

The need for absorbing boundary conditions arises when we wish to simulate problems which are naturally cast on unbounded domains. Hyperbolic problems in which features of the solution move at finite speed are limited in duration by the return of outwardly propagating features of the solution after interacting with the boundaries of the computational domain. This situation is illustrated graphically in Figure 1. Here the domain of interest is surrounded by a buffer layer whose purpose is to delay the return of the reflection. To increase the duration of validity, we must increase the size of the boundary region, with a corresponding increase in computational cost.

The perfectly matched layer and other absorbing domain methods modify the equations in the buffer region to damp the waves as they travel through it. The goal is to attenuate these waves to a level where they can be ignored when they return to the domain of interest. The computational advantages of the PML over other absorbing boundary conditions include its applicability to various numerical methods and it relative ease of implementation.

In [2], Berenger considered the problem of attaining perfect transmission of planar electromagnetic waves across a planar interface between empty space and a material half-space. This is accomplished by adding additional degrees of freedom to Maxwell's equations through a field splitting, where a single field is split into the sum of two parts which evolve according to separate equations. Subsequent

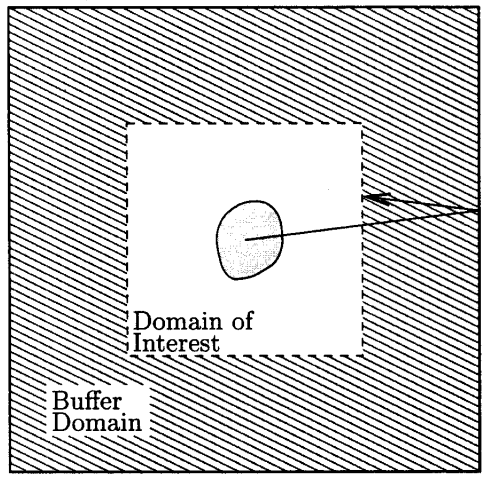

Figure 1. The layout of finite domain problems with a scattering object in the domain of interest. Note the buffer domain which delays the return of reflections to the domain on interest.

refinements of Berenger's ideas have led to new formulations of the perfectly matched layer which are demonstrably equivalent, but superior in implementation and we will pass over the details of Berenger's version in favor of another known as the anisotropic formulation. The anisotropic formulation of the perfectly matched layer is derived from Berenger's split field formulation by Mittra and Pekel in [11] and is derived directly from Maxwell's equations by Sacks, et.al. in [12] and by Gedney in [3]. We summarize the implementation for Cartesian coordinates here. The computational domain is assumed to be surrounded by PML layers of finite thickness which are backed by a conventional boundary condition, such as $\vec{E} = 0$, as illustrated in Figure 2.

For Maxwell's Equations in the frequency domain,

$$\begin{aligned} j\omega\hat{B} &= -\nabla\times\hat{E} \\ j\omega\hat{D} &= \nabla\times\hat{H} \\ \nabla\cdot\hat{B} &= 0 \\ \nabla\cdot\hat{D} &= 0 \end{aligned} \tag{1}$$

the anisotropic PML is implemented with the following constitutive

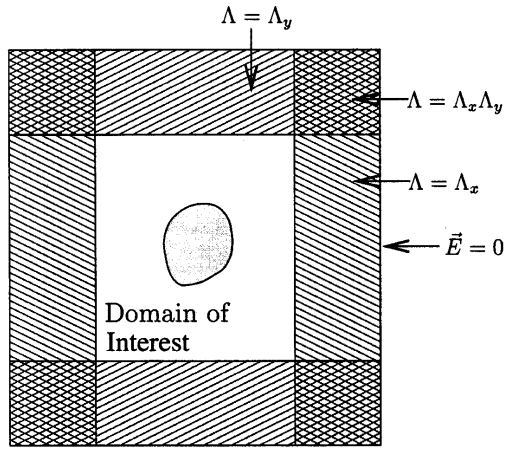

Figure 2. Diagram of a two dimensional PML application with a scattering object in the domain of interest. Note the PML boundary layers on all four sides of the computational region and the four corner regions with overlapping layers.

laws

$$\begin{aligned} \hat{D} &= \epsilon_0 \Lambda \hat{E} \\ \hat{B} &= \mu_0 \Lambda \hat{H} \end{aligned}$$

where the tensor Λ is $\Lambda = \Lambda_x \Lambda_y \Lambda_z$ and

$$\Lambda_x = \begin{pmatrix} s_x^{-1} & & \\ & s_x & \\ & & s_x \end{pmatrix}, \quad \Lambda_y = \begin{pmatrix} s_y & & \\ & s_y^{-1} & \\ & & s_y \end{pmatrix} \tag{2}$$

$$\Lambda_z = \begin{pmatrix} s_z & & \\ & s_z & \\ & & s_z^{-1} \end{pmatrix} \tag{3}$$

as obtained in [3].

The perfectly matched layer is therefore characterized by three complex numbers s_α, each moderating the absorption of waves in the particular coordinate direction α. (If attenuation of outgoing waves is not needed in a particular direction, Λ_α for that direction can be set to the identity) When each parameter is chosen to be of the form $s_\alpha = \kappa - j\beta$ we find that κ determines the wavelength of the wave in the PML and for $\beta > 0$, the wave is attenuated according to the distance

of travel in the α direction. For the interior computational domain, the constitutive laws reduce to that of free space when $s_x = s_y = s_z = 1$.

This result generalized in the obvious way for boundary layers which are matched to regions other than free space, regardless of the frequency-dependence of these parameters, (as noted in [13, p.323]), allowing us to write the general constitutive laws for perfectly matched layers which match dispersive media:

$$\begin{aligned} \hat{D} &= \epsilon(\omega)\Lambda\hat{E} \\ \hat{B} &= \mu(\omega)\Lambda\hat{H} \end{aligned}$$

This is also demonstrated in the context of a different derivation of the PML for both dispersive and anisotropic media in [15]. For our purposes, we will focus on the problem of matching PMLs to non-dispersive dielectrics. For these problems, the complete system of Maxwell's equations is:

$$\begin{aligned} j\omega\hat{B} &= -\nabla\times\hat{E} \\ j\omega\hat{D} &= \nabla\times\hat{H} \\ \hat{D} &= \epsilon\Lambda\hat{E} \\ \hat{B} &= \mu\Lambda\hat{H} \end{aligned} \tag{4}$$

When designing PMLs for time domain simulations the parameters s_α should be chosen so that the resulting frequency domain equations can be easily converted back into the time domain. The simplest of these is $s_\alpha = 1 + \sigma_\alpha/\epsilon_0 j\omega$ which we employ here. More generally, the expression $s_\alpha = \kappa_\alpha + \sigma_\alpha/\epsilon_0 j\omega$ has been used in [4] as well as $s_\alpha = 1 + \sigma_\alpha/(1 + \beta j\omega)$ in [17]. More general constitutive laws, such as the biaxial formulation in [18] have also been successfully employed.

Although the mimetic differencing schemes discussed in the next section are capable of handling discontinuous coefficients, we do not currently cast the PML equations in a form which will allow it to do so. (This may be responsible for persistent reflections which are visible in some test problems.) This difficulty arises from the frequency-dependent nature of the operator Λ and is shared by other problems with frequency dependent parameters, including ordinary dispersive materials. To reduce numerical reflections caused by discontinuous coefficients in the PML, the σ_α (and other parameters if present) are chosen to be functions of the coordinate variable α. Choosing these functions so that $s_\alpha = 1$ at the interface makes the PML a continuous extension of the medium being matched and reduces numerical reflections at the interface. Increasing the value of σ (and

possibly other coefficients) with depth in the layer allows for greater overall attenuation while keeping down the numerical reflections caused by the varying parameter. Gedney [3] suggests a conductivity profile

$$\sigma(z) = \frac{\sigma_{\max}|z - z_0|^m}{d^m} \tag{5}$$

where d is the depth of the layer, z_0 is the interface and m is the chosen power of variation. Values of m between 3 and 4 are believed to be optimal.

1.2. Expressing the PML on General Grids

The mimetic differencing scheme we will describe in Section 1.3 is capable of handling non-Cartesian two-dimensional grids. To take advantage of this flexibility, we consider the problem of expressing the PML equations in terms of an underlying grid, without reference to a particular coordinate scheme. Since we are interested in two dimensional problems, we assume homogeneity of both the problem and the underlying grid in the z direction. We will refer to the other two coordinate variables as (ξ, η) and the entire set of coordinates as (ξ, η, z).

Since the grids we wish to apply this technique to are not the result of a known transformation of the general coordinates (ξ, η) into the Cartesian coordinates (x, y). The logically rectangular nature of the grid, however, makes if possible to assign integer (ξ, η) coordinates to the nodal points and, by interpolation, to assign (ξ, η) coordinates to all points in the grid. (Generally, only the integer and integer-plus-half coordinates are used, since these give the nodes, edge centers and cell centers.) This gives an effective inverse of the coordinate transformation from the logical variables (ξ, η) to Cartesian variables. We note that when measured in these general coordinates, the length of a cell edge is always one and the width of a PML is equal to the number of cells that it covers.

We will assume that the coordinate scheme induced by the grid is orthogonal, hence we will retain the diagonal form of the PML tensor Λ. Furthermore, we assume that in the corner regions, the PML tensor factors as before into components that represent attenuation in the different coordinates, $\Lambda_\xi = \operatorname{diag}\{s_\xi^{-1}, s_\xi, s_\xi\}$, $\Lambda_\eta = \operatorname{diag}\{s_\eta, s_\eta^{-1}, s_\eta\}$, and $\Lambda_z = \operatorname{diag}\{s_z, s_z, s_z^{-1}\}$. Since we are interested in two dimensional problems in the ξ and η variables, there are no waves propagating in the z direction and we take $s_z = 1$. Hence, Λ_z is the identity matrix and will be dropped from further calculations.

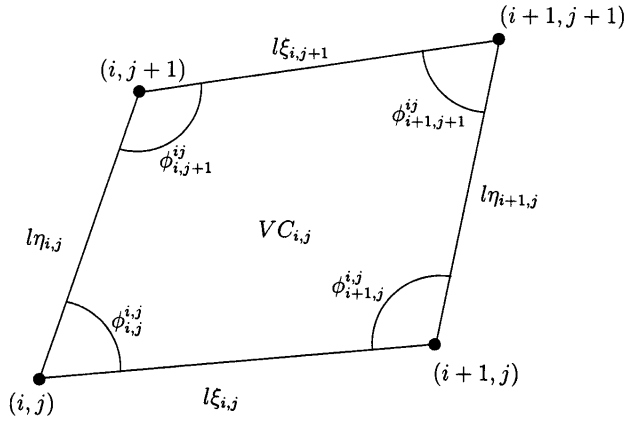

Figure 3. Cell diagram with node numbers (i, j), angles ϕ, edge lengths $l\xi, l\eta$ and cell volume VC labeled.

1.3. Background on Mimetic Difference Schemes

Mimetic Difference schemes are ones in which the discrete differential operators are chosen to mimic the properties of the continuous versions. The brief treatment here will suppress many details concerning boundary conditions and focus on the derivation of discrete curl operators. A more complete treatment can be found in [8, 7, 9]. Ref [9] specifically covers the space and time discretization for the following version of Maxwell's equations:

$$\begin{aligned} \frac{\partial \vec{B}}{\partial t} &= -\nabla \times \vec{E}, \qquad & \vec{D} &= \epsilon \vec{E} \\ \frac{\partial \vec{D}}{\partial t} &= \nabla \times \vec{H}, \qquad & \vec{B} &= \mu \vec{H} \\ \nabla \cdot \vec{D} &= 0 \\ \nabla \cdot \vec{B} &= 0. \end{aligned}$$

We consider this problem on irregular, but logically rectangular grids (i.e. Every cell has four sides and every interior node has is connected by edges to four others). At each cell in the grid, we label the nodes and specify the angles and edge lengths as given in Figure 3. We denote the space of discrete scalar functions defined on the nodes of the grid as HN and the space of discrete scalar functions defined on cell centers as HC, which are illustrated in Figure 4. We also define two spaces of

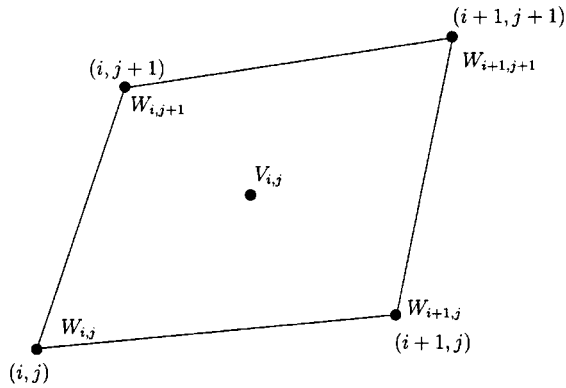

Figure 4. NH and NC space diagram. Components of scalar functions $V \in HC$ and $W \in HN$ are illustrated.

vector valued functions with components in the ξ, η and z directions. These are illustrated in Figures 5 and 6. The space $\mathcal{H}L$ consists of vector functions whose ξ, η components which are tangential to the edges of the grid and whose z components are defined at the grid nodes. Likewise, the space $\mathcal{H}S$ consists of functions whose ξ, η components are defined normal to the cell edges and whose z components are defined at cell centers. (We note that in three dimensions, all of the components of $\mathcal{H}L$ and $\mathcal{H}S$ functions are defined on cell edges and the centers of cell faces. The two dimensional version here is obtained by projecting a three dimensional grid which is uniform in the z direction onto the ξ, η plane.)

For the problems that we are interested in, we approximate the unknown vector quantities $\vec{E}$ and $\vec{D}$ with discrete versions in $\mathcal{H}L$ and $\vec{H}$ and $\vec{B}$ with discrete versions in $\mathcal{H}S$. The unknowns appear on the grid as illustrated in Figure 7. Here, we note the similarity to the Yee scheme [19] for computational electromagnetics in two dimensions, as each component of the electric field is surrounded by circulating components of the magnetic field and vice versa. We also note that the electric field and flux are tangential to the grid lines while the magnetic field and flux are normal to them. This has implications for the choice of independent variables when dealing with discontinuities in material parameters and which boundary conditions can be readily implemented.

We define the *natural operators* to act on these spaces of discrete functions. DIV : $\mathcal{H}S \mapsto HC$, GRAD : $HN \mapsto \mathcal{H}L$ and CURL : $\mathcal{H}L \mapsto$

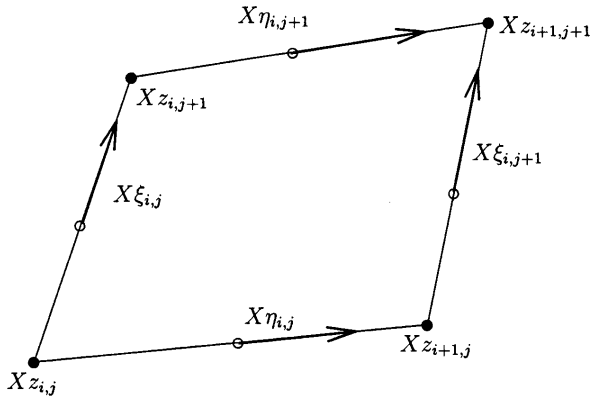

Figure 5. $\mathcal{H}L$ space diagram. Components of a vector function $\vec{X} \in \mathcal{H}L$ are illustrated.

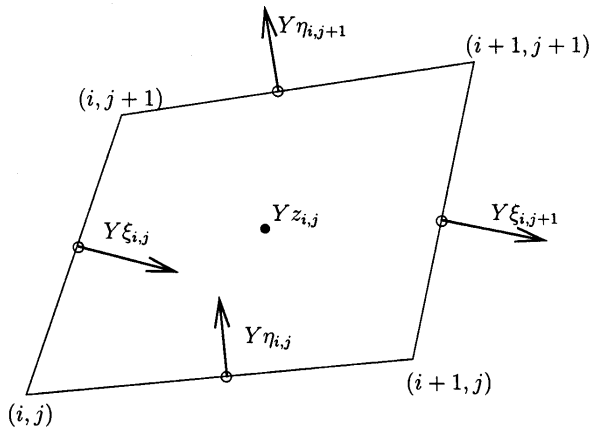

Figure 6. $\mathcal{H}S$ space diagram. Components of a vector function $\vec{Y} \in \mathcal{H}S$ are illustrated.

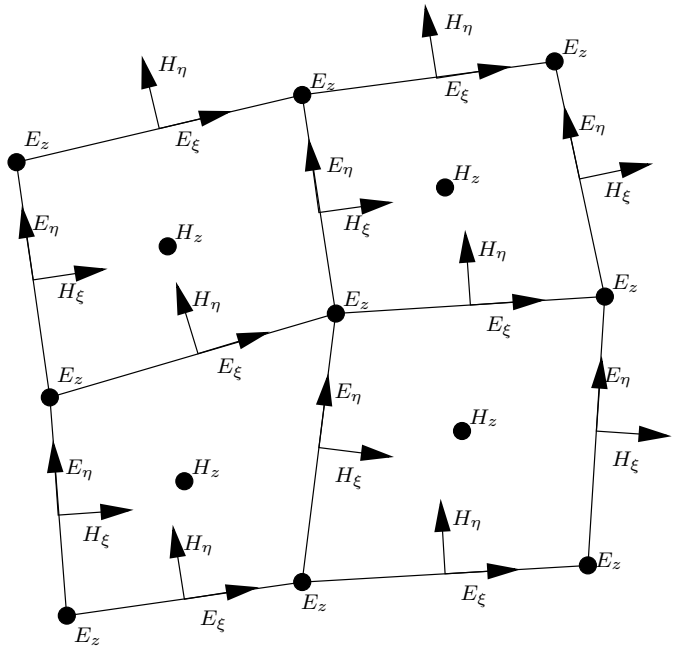

Figure 7. Layout of field components on irregular, logically-rectangular grid. Electric field components are defined tangent to edges and at nodes. Magnetic field components are defined normal to edges and at cell centers.

$\mathcal{H}S$. These operators are constructed so that they satisfy the major theorems of differential operators, including $\mathrm{DIV}\vec{A} = 0$ if and only if $\vec{A} = \mathrm{CURL}\,\vec{B}$ and $\mathrm{CURL}\,\vec{A} = 0$ if and only if $\vec{A} = \mathrm{GRAD}\phi$ (see [8] for details). The expressions for the DIV and GRAD operators resemble the standard finite volume operators are are straightforward to derive. Since it is of the most interest here, we give the definition of CURL in more detail. If $\vec{R} = (R\xi, R\eta, Rz)^T = \mathrm{CURL}\,\vec{E}$ then

$$R\xi_{i,j} = \frac{Ez_{i,j+1} - Ez_{i,j}}{l\eta_{i,j}}, \quad R\eta_{i,j} = \frac{Ez_{i+1,j} - Ez_{i,j}}{l\xi_{i,j}} \tag{6}$$

$$\begin{aligned} Rz_{i,j} &= \{(E\eta_{i+1,j} l\eta_{i+1,j} - E\eta_{i,j} l\eta_{i,j}) \\ &- (E\xi_{i,j+1} l\xi_{i,j+1} - E\xi_{i,j} l\xi_{i,j})\}/VC_{i,j}. \end{aligned}$$

We note that the set of natural operators is not sufficient for our discrete Maxwell's equations. Specifically, the CURL operator, since

it is defined on $\mathcal{H}L$, cannot be applied to the vector function $H \in \mathcal{H}S$. In addition, there is no grad operator for scalar functions on HC or divergence operator for vector functions on $\mathcal{H}L$. This prevents their composition to form discrete Laplace operators. The *support operator method* described in [7] is used to define new operators $\overline{\mathrm{DIV}}$, $\overline{\mathrm{GRAD}}$ and $\overline{\mathrm{CURL}}$ which are adjoints to the natural operators above and act on different spaces of functions. Roughly, the procedure is as follows:

(i) A discrete form of the *natural inner product* is defined for the various spaces of discrete functions. Each of these are then related to simpler *formal inner product* for each space through the action of symmetric linear operators.

(ii) The *formal adjoints* of the natural operators are derived. These are the adjoints with respect to the formal inner products on each space.

(iii) The adjoint operators $\overline{\mathrm{DIV}}$, $\overline{\mathrm{GRAD}}$ and $\overline{\mathrm{CURL}}$ are defined as the adjoints of the operators DIV , GRAD and CURL with respect to the natural inner products.

(iv) Computational expressions are derived for the adjoint operators using the formal adjoints and the transformations between the natural and formal inner products.

In our development here, we will focus on the derivation of the adjoint operator $\overline{\mathrm{CURL}}$. To simplify the expressions for the inner products, we restrict our attention to functions which are zero on the boundary of the grid.

For the discrete space of vector functions $\mathcal{H}S$, the formal inner product is

$$[\vec{A},\vec{B}]_{\mathcal{H}S} = \sum_{f\xi\in\mathcal{H}S\xi} A\xi_{f\xi}B\xi_{f\xi} + \sum_{f\eta\in\mathcal{H}S\eta} A\eta_{f\eta}B\eta_{f\eta} + \sum_{fz\in\mathcal{H}Sz} Az_{fz}Bz_{fz}. \tag{7}$$

Here, $f\xi, f\eta$ and fz are multi-indices for the corresponding families of cell components. $\mathcal{H}S\xi$ and $\mathcal{H}S\eta$ are cell edges, while $\mathcal{H}Sz$ are the cell centers. To define a natural inner product for the space $\mathcal{H}S$, we first define an approximation to the inner product of two members of $\mathcal{H}S$ on a given cell:

$$\begin{aligned}(\vec{A},\vec{B})_{i,j} = &\sum_{k,l=0}^{1} \frac{V^{i,j}_{i+k,j+l}}{\sin^2\phi^{i,j}_{i+k,j+l}} \\ &\cdot[A\xi_{(i+k,j)}B\xi_{(i+k,j)} + A\eta_{(i,j+l)}B\eta_{(i,j+l)} \\ &+(-1)^{k+l}(A\xi_{(i+k,j)}B\eta_{(i,j+l)}A\eta_{(i,j+l)}B\xi_{(i+k,j)})\cos\phi^{(i,j)}_{(i+k,j+l)}] \\ &+Az_{ij}Bz_{ij},\end{aligned} \tag{8}$$

where the weights $V^{(i,j)}_{(i+k,j+l)}$ satisfy

$$V^{(i,j)}_{(i+k,j+l)} \geq 0, \quad \sum_{k,l=0}^{1} V^{(i,j)}_{(i+k,j+l)} = 1. \tag{9}$$

Note that each (k,l) pair corresponds to a corner of the (i,j)th cell and that the weights have the same notation as the cell angles. For our computations, we base the weights on the area of the triangle made by each angle and the two adjacent sides, normalized to satisfy the conditions in (9). The natural inner product for space $\mathcal{H}S$ is then defined

$$(\vec{A},\vec{B})_{\mathcal{H}S} = \sum_{c} (\vec{A},\vec{B})_c VC_c \tag{10}$$

where c is the multi-index over all cells in the grid and VC_c is the area of cell c.

This process is repeated for the $\mathcal{H}L$ space, with results similar to equations (7), (8) and (10). By examining the definitions of the formal and natural inner products for these spaces, we construct symmetric positive operators $\mathcal{S} : \mathcal{H}S \mapsto \mathcal{H}S$ and $\mathcal{L} : \mathcal{H}L \mapsto \mathcal{H}L$ such that

$$(\vec{A},\vec{B})_{\mathcal{H}S} = [\mathcal{S}\vec{A},\vec{B}]_{\mathcal{H}S}, \quad (\vec{A},\vec{B})_{\mathcal{H}L} = [\mathcal{L}\vec{A},\vec{B}]_{\mathcal{H}L} \tag{11}$$

Let $\mathrm{CURL}^\dagger$ denote the *formal adjoint* of CURL, i.e., the adjoint with respect to the formal inner product: $[\,\mathrm{CURL}\,\vec{A},\vec{B}]_{\mathcal{H}S} = [\vec{A},\,\mathrm{CURL}^\dagger\,\vec{B}]_{\mathcal{H}L}$. We can verify directly that if $\vec{R} = \,\mathrm{CURL}^\dagger\,\vec{B}$ then

$$R\xi_{ij} = -l\xi_{ij}\left(\frac{Bz_{(i,j-1)}}{VC_{(i,j-1)}} - \frac{Bz_{ij}}{VC_{ij}}\right), \quad R\eta_{ij} = l\eta_{ij}\left(\frac{Bz_{(i-1,j)}}{VC_{(i-1,j)}} - \frac{Bz_{ij}}{VC_{ij}}\right) \tag{12}$$

$$Rz_{ij} = \left(\frac{B\xi_{(i,j-1)}}{l\eta_{(i,j-1)}} - \frac{B\xi_{ij}}{l\eta_{ij}}\right) - \left(\frac{B\eta_{(i-1,j)}}{l\xi_{(i-1,j)}} - \frac{B\eta_{ij}}{l\xi_{ij}}\right) \tag{13}$$

We define the operator $\overline{\mathrm{CURL}}$ as the adjoint of CURL with respect to the natural inner products on $\mathcal{H}L$ and $\mathcal{H}S$. Hence, $\overline{\mathrm{CURL}} : \mathcal{H}S \mapsto \mathcal{H}L$ and for all $\vec{A} \in \mathcal{H}L, \vec{B} \in \mathcal{H}S$

$$(\,\mathrm{CURL}\,\vec{A},\vec{B})_{\mathcal{H}S} = (\vec{A},\,\overline{\mathrm{CURL}}\,\vec{B})_{\mathcal{H}L} \tag{14}$$

Using the definitions and symmetry of the operators $\mathcal{L}$, $\mathcal{S}$ in (11), we find that $\mathcal{L}\,\overline{\mathrm{CURL}}\,\vec{B} = \,\mathrm{CURL}^\dagger\,\mathcal{S}\vec{B}$. Expressed as an operator, we define $\overline{\mathrm{CURL}}$ by $\overline{\mathrm{CURL}} = (\mathcal{L})^{-1}\,\mathrm{CURL}^\dagger\,\mathcal{S}$.

Repeating this procedure for DIV and GRAD as detailed in [7], generates the operators $\overline{\text{DIV}} : \mathcal{H}L \mapsto HN$ and $\overline{\text{GRAD}} : HC \mapsto \mathcal{H}S$. These new operators also satisfy the same discrete versions of vector calculus theorems as the natural operators. Furthermore, with these operators, all of the following composite operators can be formed as well:

$$\begin{array}{cc} \text{DIV } \overline{\text{GRAD}} : HC \to HC & \overline{\text{DIV}} \text{ GRAD} : HN \to HN \\ \text{CURL } \overline{\text{CURL}} : \mathcal{H}S \to \mathcal{H}S & \overline{\text{CURL}} \text{ CURL} : \mathcal{H}L \to \mathcal{H}L \\ \text{GRAD } \overline{\text{DIV}} : \mathcal{H}L \to \mathcal{H}L & \overline{\text{GRAD}} \text{ DIV} : \mathcal{H}S \to \mathcal{H}S \end{array}$$

1.4. Application of Mimetic Difference Operators to Maxwell's Equations

From the integral form of Maxwell's equations (see, for example [10, Section 1.5] or [1, Section 1.5]) we find that at discontinuous material interfaces the tangential components of the fields $\vec{E}$ and $\vec{H}$ are continuous while the normal components of the flux densities $\vec{D}$ and $\vec{B}$ are continuous. Given that material interfaces will occur along grid lines in the the discrete problem and the location of the discrete field components on the grid, the quantities E and B are continuous in our formulation, while D and H are not. Hence, before discretizing Maxwell's equations, we express them in terms of these continuous quantities.

$$\begin{aligned} \frac{\partial \vec{B}}{\partial t} &= -\nabla \times \vec{E} \\ \frac{\partial \vec{E}}{\partial t} &= \frac{1}{\epsilon} \nabla \times \frac{1}{\mu} \vec{H} \end{aligned}$$

This leads to the derivation of the slightly different adjoint operator ${}_{\epsilon}\overline{\text{CURL}}_{\mu}$ corresponding to the continuous operator $\frac{1}{\epsilon}\nabla \times \frac{1}{\mu}$. Weighted inner products based on the parameters ϵ and μ are used for the spaces $\mathcal{H}L$ and $\mathcal{H}S$, resulting in new operators $\mathcal{L}^{\epsilon}$ and $\mathcal{S}^{1/\mu}$. Then, with respect to these weighted norms,

$$(\text{ CURL } \vec{A}, \vec{B})^{\epsilon}_{\mathcal{H}S} = (\vec{A}, \overline{\text{CURL}}\, \vec{B})^{\frac{1}{\mu}}_{\mathcal{H}L}. \tag{15}$$

The derivation of the operators $\mathcal{L}^{\epsilon}$ and $\mathcal{S}^{1/\mu}$ are detailed in [9]. The case where ϵ and μ are symmetric positive-definite tensors is handled in [6]. Using these operators, the discrete form of Maxwell's equations

is now

$$\begin{aligned} \frac{\partial \vec{B}}{\partial t} &= -\operatorname{CURL} \vec{E} \\ \frac{\partial \vec{E}}{\partial t} &= {}_{\epsilon}\overline{\operatorname{CURL}}_{\mu} \vec{H}. \end{aligned}$$

2. IMPLEMENTATION

2.1. Combining the PML Equations and Mimetic Difference Operators

To cast our system of Maxwell's equations plus PML equations into the form appropriate for the mimetic difference operators from Section 1.4, we return to the frequency domain equations (4) and define the following new field values:

$$\hat{E}_p = \Lambda \hat{E} \tag{16}$$

$$\hat{B}_p = \Lambda^{-1} \hat{B}. \tag{17}$$

Maxwell's equations are now

$$j\omega \hat{B} = -\nabla \times \hat{E} \tag{18}$$

$$j\omega \hat{E}_p = \frac{1}{\epsilon} \nabla \times \frac{1}{\mu} \hat{B}_p \tag{19}$$

with the new constitutive laws

$$\begin{aligned} \hat{D} &= \epsilon \hat{E}_p \\ \hat{B}_p &= \mu \hat{H}. \end{aligned}$$

Equations (16)–(19) form a fully determined dynamical system in the variables E, B, E_p, B_p when converted back into the time domain. The explicit form of the time domain equations will be covered in the next section in the context of general systems of coordinates.

We also note here that because of the change in field values, the quantities which appear in equation (19) are not necessarily continuous at a material interface. We will attempt to alleviate this this problem by choosing the parameters which appear in Λ to be continuous as discussed in Section 1.1.

2.2. Conversion to the Time Domain

Maxwell's equations (18, 19) as derived in the previous section, can be converted back into the time domain as discretized in space to yield

$$\begin{aligned} \frac{\partial B}{\partial t} &= -\,\mathrm{CURL}\, E \\ \frac{\partial E_p}{\partial t} &= {}_{\epsilon}\overline{\mathrm{CURL}}_{\mu} B_p. \end{aligned}$$

The remaining equations all arise from the PML are involve no space derivatives.

$$\begin{aligned} \hat{E} &= \Lambda_\eta^{-1}\Lambda_\xi^{-1}\hat{E}_p \\ \hat{B}_p &= \Lambda_\eta^{-1}\Lambda_\xi^{-1}\hat{B} \end{aligned}$$

In our simulations, we consider the transverse electric (TE) mode, which consists of the components E_ξ, E_η and B_z. Dropping the equations in which all components are zero and using the definitions of the matrices Λ_ξ and Λ_η yields the equations:

$$E_\xi = s_\xi s_\eta^{-1} E_\xi^p \tag{20}$$

$$E_\eta = s_\xi^{-1} s_\eta E_\eta^p \tag{21}$$

$$B_z = s_\xi^{-1} s_\eta^{-1} B_z^p \tag{22}$$

where E_ξ^p, E_η^p, B_z^p are components of E_p and B_p. Equations (20) and (21) have the general form

$$X s_\alpha = Y s_\beta \tag{23}$$

where a_α and s_β are two different complex PML coefficients and X, Y are vector field components. We illustrate the exact procedure for converting equations of this type into the time domain for $s_\alpha = \kappa_\alpha + \sigma_\alpha/\epsilon_0 j\omega$. Equation (23) becomes

$$\left(\kappa_\alpha + \frac{\sigma_\alpha}{\epsilon_0 j\omega}\right) X = \left(\kappa_\beta + \frac{\sigma_\beta}{\epsilon_0 j\omega}\right) Y$$

Multiplying by $j\omega$ and converting, we obtain,

$$\kappa_\alpha \frac{\partial X}{\partial t} + \frac{\sigma_\alpha}{\epsilon_0} X = \kappa_\beta \frac{\partial Y}{\partial t} + \frac{\sigma_\beta}{\epsilon_0} Y. \tag{24}$$

Given that one of the two quantities, $\frac{\partial X}{\partial t}, \frac{\partial Y}{\partial t}$ is determined by other equations in the dynamical system, (24) can then be solved for the remaining unknown time derivative.

To discretize equation (22) we introduce an intermediate variable, $\bar{B}_z^p$ and split it into two equations:

$$\begin{aligned} s_\xi B_z &= \bar{B}_z^p \\ s_\eta \bar{B}_z^p &= B_z^p. \end{aligned} \tag{25}$$

These equations can be converted to the time domain by the same process. For our expanded system consisting of $E_\xi, E_\eta, E_\xi^p, E_\eta^p, B_z, B_z^p$ and $\bar{B}_z^p$, the resulting system of time-domain equations is:

$$\frac{\partial \vec{B}}{\partial t} = -\,\mathrm{CURL}\,\vec{E} \tag{26}$$

$$\frac{\partial \vec{E}_p}{\partial t} = {}_\epsilon\overline{\mathrm{CURL}}_\mu \vec{B}_p \tag{27}$$

$$\frac{\partial E_\xi}{\partial t} = \frac{1}{\kappa_\eta}\left(\sigma_\xi E_\xi^p - \sigma_\eta E_\xi + \kappa_\xi \frac{\partial E_\xi^p}{\partial t}\right) \tag{28}$$

$$\frac{\partial E_\eta}{\partial t} = \frac{1}{\kappa_\xi}\left(\sigma_\eta E_\eta^p - \sigma_\xi E_\eta + \kappa_\eta \frac{\partial E_\eta^p}{\partial t}\right) \tag{29}$$

$$\frac{\partial \bar{B}_z^p}{\partial t} = \sigma_\xi B_z + \kappa_\xi \frac{\partial B_z}{\partial t} \tag{30}$$

$$\frac{\partial B_z^p}{\partial t} = \sigma_\eta \bar{B}_z^p + \kappa_\eta \frac{\partial \bar{B}_z^p}{\partial t} \tag{31}$$

The equations (26), (27) are vector equations for all three components of $\vec{E}$, $\vec{B}$, $\vec{E}_p$ and $\vec{B}_p$. Our TE mode solution only involves three of these six equations. The remaining time derivatives in the right-hand-sides of equations (28) through (31) can be eliminated through substitution.

2.3. Discretization of the Equations

We employ the same staggered time-stepping approach as proposed by Yee [19]. In this scheme, the values of the electric field and related quantities are updated at integer multiples of the fundamental time step while the magnetic field and related quantities are updated at the midpoints of the intervals, denoted with the indices $n + 1/2$. Forward differencing schemes are used for each step of the process with second order convergence of the results in time. For our implementation, the quantities $E_\xi, E_\eta, E_\xi^p, E_\eta^p$ are defined on the integral multiples of the time step n. The quantities B_z, B_z^p and $\bar{B}_z^p$ are defined on the midpoints $n + \frac{1}{2}$.

The discrete form of the equations that we implement here is not derived directly from the system of equations (26)–(31). Instead, we discretize all of the expressions in the form of equation (24) and equations (25) directly using standard first-order differences for the time derivatives and the two-point average for the conductivity terms. This yields the following update equation for the discrete quantities:

$$X^{n+1}\left(\frac{\sigma_\alpha}{2}+\frac{\kappa_\alpha}{\Delta t}\right)+X^n\left(\frac{\sigma_\alpha}{2}-\frac{\kappa_\alpha}{\Delta t}\right)=Y^{n+1}\left(\frac{\sigma_\beta}{2}+\frac{\kappa_\beta}{\Delta t}\right)+Y^n\left(\frac{\sigma_\beta}{2}-\frac{\kappa_\beta}{\Delta t}\right). \tag{32}$$

One of the $n+1$ terms is already known from it's involvement in other equations, so this expression is solved for the unknown $n+1$ term. (The equation for quantities on the half time intervals is found by adjusting the indices.)

The main loop of the iteration, illustrating the mutual dependencies of the data, is as follows. We start with current values at the time steps n and $n-\frac{1}{2}$. Unless otherwise stated, the update rule is some form of equation (32).

- Compute $B_z^{n+\frac{1}{2}}$ from $B_z^{n-\frac{1}{2}}$ and E_x^n, E_y^n from $Bz^{n+\frac{1}{2}} = Bz^{n-\frac{1}{2}} - \Delta t(\,\mathrm{CURL}\,E)_z$.
- Compute $\bar{B}_z^{p,n+\frac{1}{2}}$ from $\bar{B}_z^{p,n-\frac{1}{2}}$, $B_z^{n-\frac{1}{2}}$ and $B_z^{n+\frac{1}{2}}$.
- Compute $B_z^{p,n+\frac{1}{2}}$ from $B_z^{p,n-\frac{1}{2}}$, $\bar{B}_z^{p,n-\frac{1}{2}}$ and $\bar{B}_z^{p,n+\frac{1}{2}}$.
- Compute $E_x^{p,n+1}$ and $E_y^{p,n+1}$ from $E_x^{p,n}, E_y^{p,n}$ and $B_z^{p,n+\frac{1}{2}}$ from $\vec{E}^{p,n+1} = \vec{E}^{p,n} + \Delta t\,{}_\epsilon\overline{\mathrm{CURL}}_\mu \vec{B}^p$.
- Compute E_x^{n+1} from E_x^n, $E_x^{p,n}$ and $E_x^{p,n+1}$.
- Compute E_y^{n+1} from E_y^n, $E_y^{p,n}$ and $E_y^{p,n+1}$.

3. TEST PROBLEMS AND RESULTS

3.1. Radiation Problem on a Cartesian Grid

Our first test problem uses a small current loop in the $\xi\eta$ plane, implemented as a fictitious magnetic current, to generate a TE mode electromagnetic pulse. The magnetic current for this and other examples below has the Gaussian time signature:

$$f(t) = e^{-(t-t_c)^2/w^2} \tag{33}$$

and in this example, we take $t_c = 1.0 \times 10^{-10}$ and $w = 2.5 \times 10^{-11}$. (We note that at $t = 0$, $f(0) = e^{-16} \approx 1.1 \times 10^{-7}$ so we need not worry

about the initial discontinuity.) The current source is placed at $(0, 0)$ in a square domain $[-0.024, 0.024] \times [-0.024, 0.024]$ and the z component of the magnetic field is observed at the point $(-0.012, 0.012)$ (chosen because it lies exactly on one of the grid points). The grid covering the domain is 60 elements square and the PMLs are ten grid elements wide. The power of variation of σ (see (5)) is $m = 4$. The result of several different simulations with various values of $\sigma_{\max}$ are plotted in Figure 8.

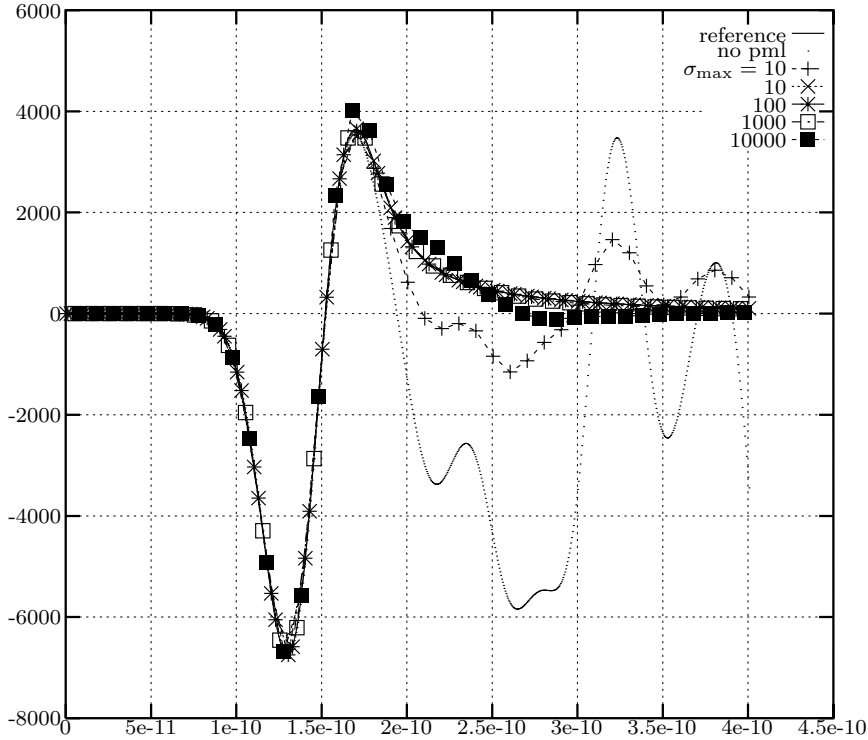

Figure 8. Observed Magnetic field in radiation problem on Cartesian grid. PML layers with $\sigma_{\max}$ between 10 and 1000 give good agreement with reference solution.

The reference domain plot in Figure 8 is computed without an absorbing boundary layer on a domain sufficiently large so that the simulation ends before the return of reflections from the boundary. We can see that for a wide range of $\sigma_{\max}$ the PML is highly effective. We also tested the long-term stability of the method by running it to 100,000 time steps. No late time instability was observed.

We repeat this experiment on the grid in Figure 9 which has been distorted in the interior of the domain, but not in the region occupied by the PMLs. The dimensions and input signal are identical to the previous example and the results of the simulation are displayed in Figure 10. As before, we see that the agreement between the reference solution and the PML solution is quite good.

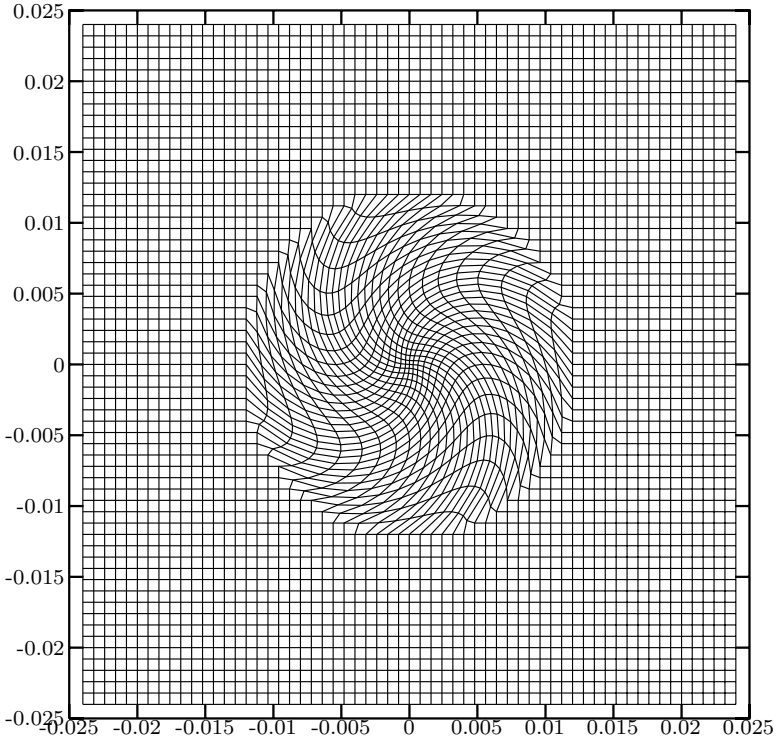

Figure 9. Plot of modified square grid. Note non-orthogonality of grid in the interior, away from PML layers on the four sides.

In both of these examples, the grid lines within the PML are aligned with the x and y axes. To demonstrate the effectiveness of the our formulation in which the PML properties are defined with respect to the grid and not the Cartesian coordinate system, we repeated this experiment on Cartesian grids rotated at various angles to the origin. For example, the grid in Figure 11 rotated through an angle of 35^o. In all tested problems of this sort the PML performed identically to the PML on the original, unrotated grid.

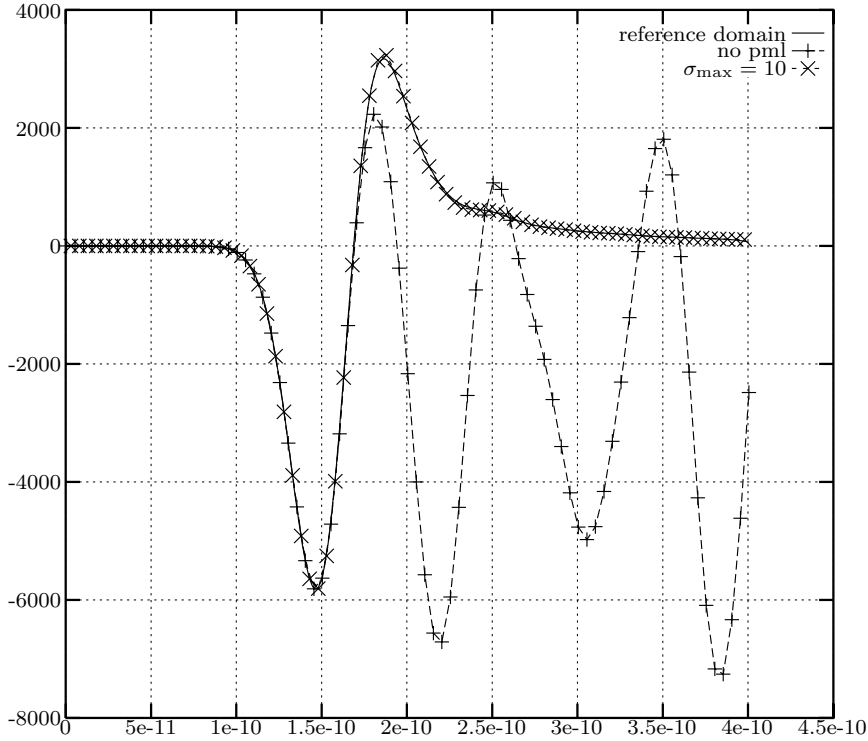

Figure 10. Observed Magnetic field in radiation problem on modified grid. Results agree with both reference domain solution and results on unmodified grid.

3.2. Scattering Problem on a Polar Grid

Here, we simulate the reflection of a Gaussian plane-wave pulse off a perfectly conducting cylinder of radius 0.1 meter. Traveling TE mode plane-waves have the following general form:

$$B_z = f\left(t - \frac{1}{c}\vec{x}\cdot\vec{k}\right) \tag{34}$$

$$E_x = -\eta_0 k_y f\left(t - \frac{1}{c}\vec{x}\cdot\vec{k}\right) \tag{35}$$

$$E_y = \eta_0 k_x f\left(t - \frac{1}{c}\vec{x}\cdot\vec{k}\right) \tag{36}$$

which can be seen to satisfy Maxwell's equations by substitution. We choose the Gaussian pulse from equation (33) with $t_c = 1.0 \times 10^{-9}$,

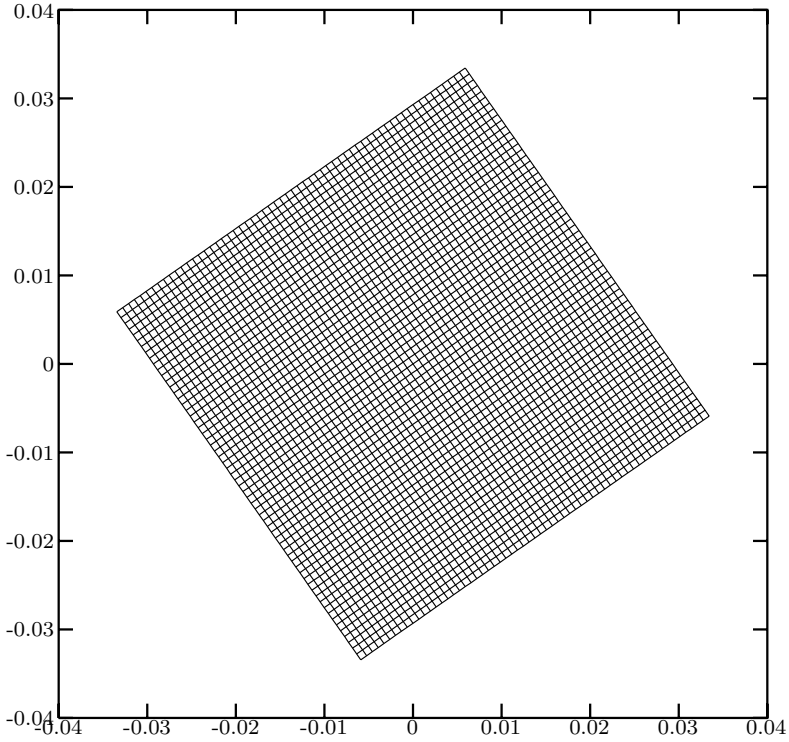

Figure 11. Rotated Cartesian grid. This demonstrates the effectiveness of the coordinate-free formulation of the PML.

$w = 2.0 \times 10^{-10}$ for the wave-shape function f. We also pick the wave vector $\vec{k} = (1, 0, 0)$, representing a pulse traveling to the right along the x axis. Using the symmetry of the problem and the source terms, we compute the scattered field only in the positive y half-plane on the polar grid in Figure 12. There are 40 divisions of the angular coordinate θ and 61 divisions of the radius r.

The inner semi-circle at $r = 0.1$ is the surface of the conducting cylinder where the boundary conditions on the electric field are imposed. The total electric field is zero at the surface of the conducting cylinder, thus

$$\vec{E}_{\text{reflected}} = -\vec{E}_{\text{incident}} \tag{37}$$

where the incident field is given by the equations (35) and (36). Since $\vec{E}$ is defined along cell edges, we impose this condition on the inner semi-circle of edges which represent the surface of the cylinder by computing the projection of $\vec{E}_{\text{incident}}$ onto each edge and using (37).

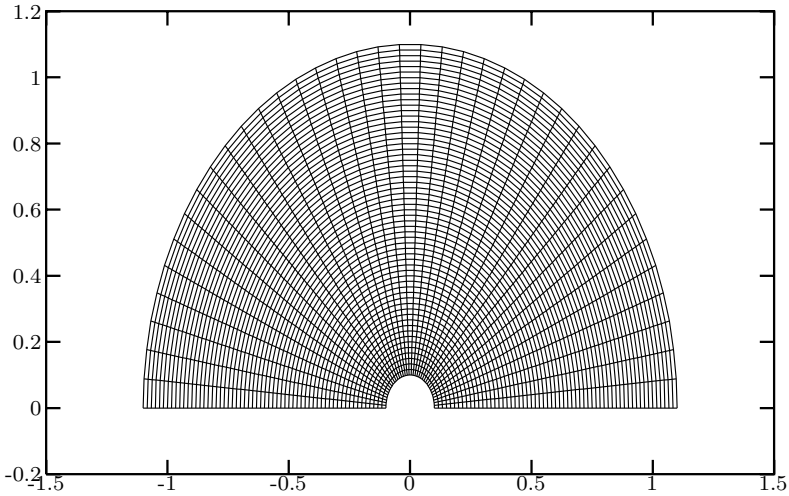

Figure 12. Polar grid used in reflecting cylinder problem. The conducting cylinder is the inner semicircular boundary. A PML layer is placed on the outer semicircular boundary.

For boundary conditions on the remaining three boundaries we set the tangential electric field components to zero. The symmetry of the problem implies this condition along the edges at $\theta = 0$ and $\theta = \pi$. The boundary at $r = 1.1$ is covered with a a perfectly matched layer of various cell widths.

Although we use the polar coordinates (r, θ) to describe the layout of the problem, we do not use an explicit coordinate transformation from Cartesian coordinates or a polar coordinates version of Maxwell's equations (as discussed in Section 1.2) instead treating it as a problem on a general grid. PML formulations made directly in cylindrical coordinates (for example, see [16] or [18]) are applicable to this problem and yield a different PML tensor then the one we use here. In [14] it is shown that the tensor component

$$\Lambda_r = \mathrm{diag}\left\{\frac{\tilde{r}}{r}\frac{1}{s_r}, \frac{r}{\tilde{r}}s_r, \frac{\tilde{r}}{r}s_r\right\}$$

yields a perfectly matched PML in the continuous limit. Here $\tilde{r}$ is a complex stretched coordinate version of the radial parameter. The version of the tensor that we use here, $\mathrm{diag}\{\frac{1}{s_r}, s_r, s_r\}$ is known as a *Quasi-PML* [5] and is not perfectly reflecting in the continuous limit because of the missing factors of $\frac{\tilde{r}}{r}$.

Numerical experiments show the limitations of the effectiveness of the quasi-PML formulation applied to this problem. A typical result is illustrated in Figure 13. Here, the depth of the PML is held constant while the maximum σ value varies over the range $(0.5, 10)$. The power of σ variation is again $m = 4$. In Figure 14 we examine more closely the time interval in which the reflection appears and find that it is constant over a wide range of $\sigma_{\max}$ values. This reflection also appears in other simulations in which we refine the spatial discretization, refine the time discretization and increase the depth of the layer, indicating that it is due solely to the imperfect matching of the quasi-PML. By running each of these simulations to 30,000 time steps we also verified the late-time stability of the scheme.

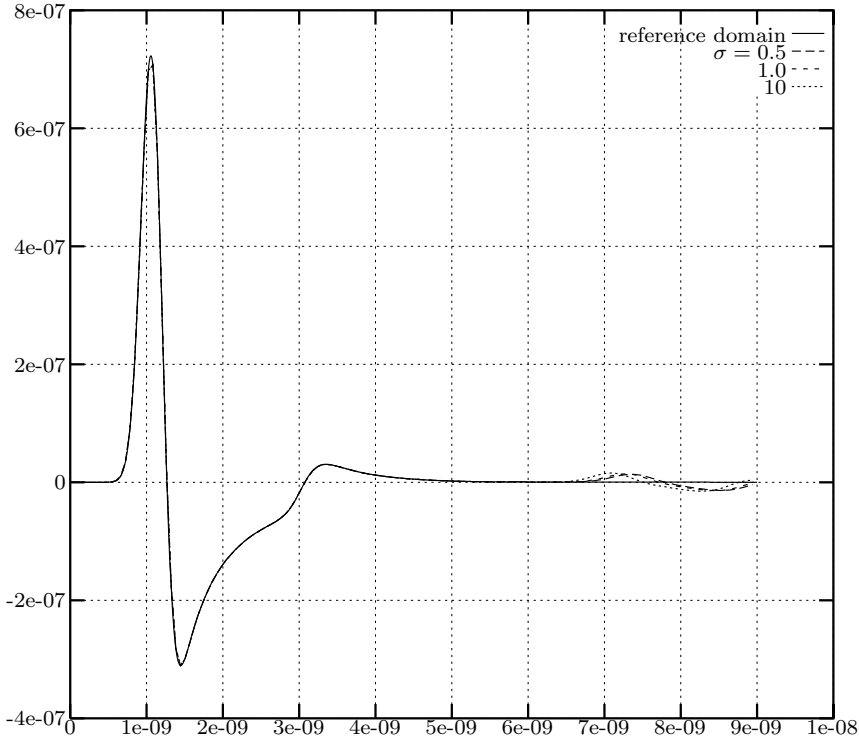

Figure 13. Results on the polar grid for the reflecting cylinder with PMLs at various $\sigma_{\max}$. Note the systematic discrepancy between these and the reference solution.

We note that the discrete form of the cylindrical grid is only approximately orthogonal because of the straight edges between nodes

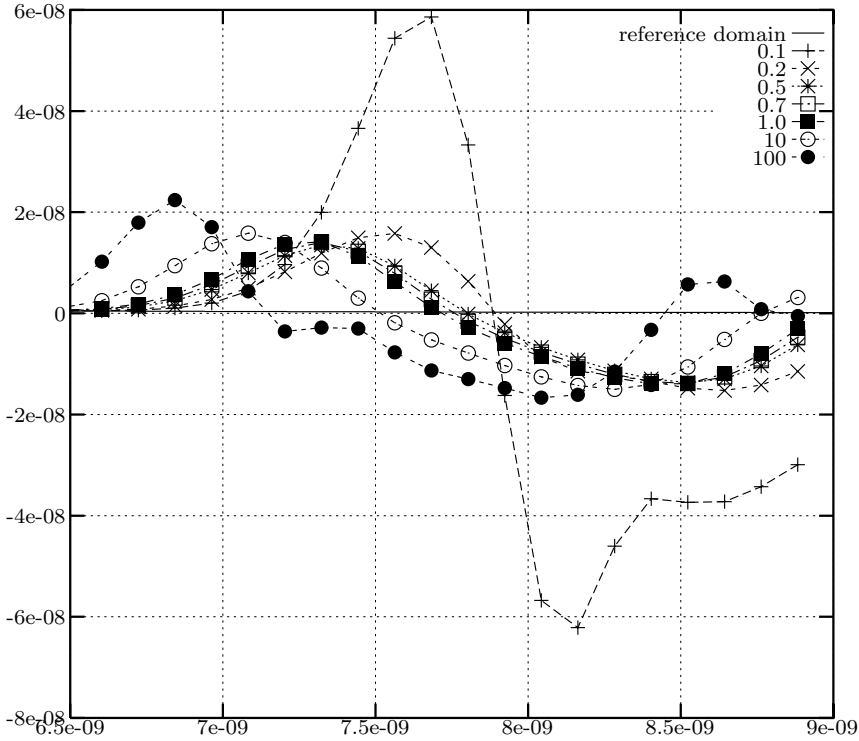

Figure 14. Close up of the results in Figure 13. Note the consistent size of the discrepancy for $\sigma_{\max} = 0.2$ to $\sigma_{\max} = 10$.

on the grid. This makes the angles between the radial (ξ) and angular (η) coordinates different from 90°. By forcing the angles to be 90° in the computation of the operators CURL and ${}_{\epsilon}\overline{\mathrm{CURL}}_{\mu}$, as described in Section 1.4, we improve the approximation of an orthogonal grid. The simulation results with the modified operators are nearly identical to the one implementing the correct cell angles, including the performance of the PML.

3.3. Skew Grid

To test the dependence of the PML performance on the orthogonality of the grid, we employ it on grids with increasing degrees of nonorthogonality like the one in Figure 15. We demonstrate that the same perfectly matched layer performs progressively worse as the nonorthogonality of the grid increases. Each of these grids has a ten cell

wide PML layer on the top, bottom and right boundaries. A traveling wave with the same Gaussian shape as in the previous examples and moving in the positive x direction is generated through the boundary conditions on the top and bottom of the grid. (That this method works despite the presence of the PML layers on the top and bottom demonstrates the fact that the PML does not attenuate waves which propagate transverse to its depth direction.) The B_z field component is observed in each example at the point $(0.25, 0.5)$

We present graphically results on two different skew grids. The first example uses the slightly skewed square grid in Figure 15. The results of simulations with and without PML layers is in Figure 16.

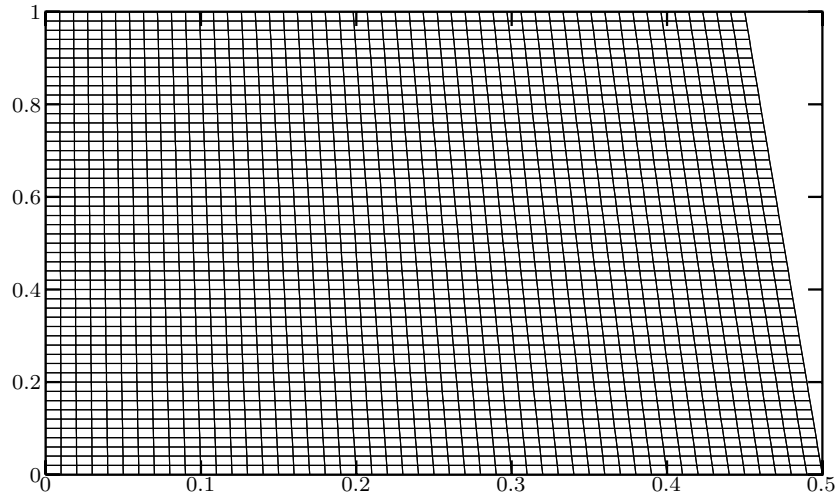

Figure 15. Slightly skew grid.

We can see that the PML absorbs most of the pulse, leaving a reflection roughly two orders of magnitude smaller. Although still small, this reflection is far larger than those from PMLs on orthogonal grids. On the grid in Figure 17 where the coordinate lines are more nonorthogonal, the PML performs considerably worse, as shown in Figure 18.

4. CONCLUSIONS

We have created a perfectly matched layer implementation based on the anisotropic tensor formulation and discretized with a mimetic

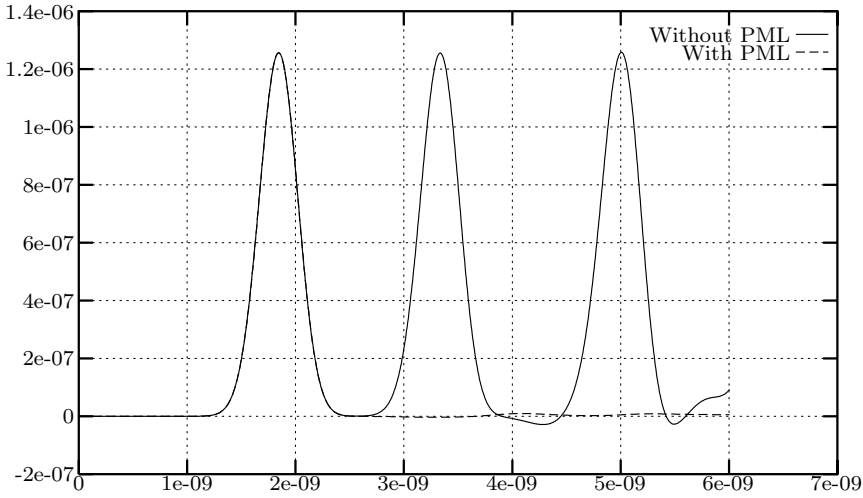

Figure 16. Observed magnetic field with and without PML on the slightly skew grid of Figure 15. Note that the reflections apparent with the PML are small compared the other pulse size.

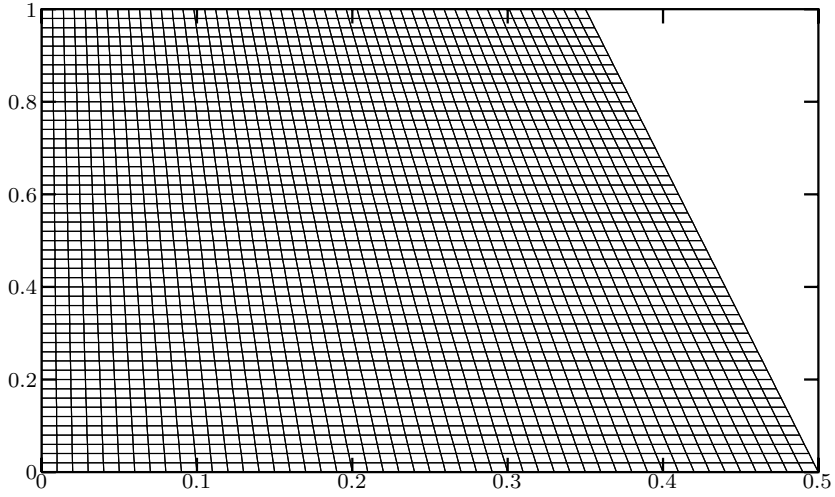

Figure 17. Skew grid.

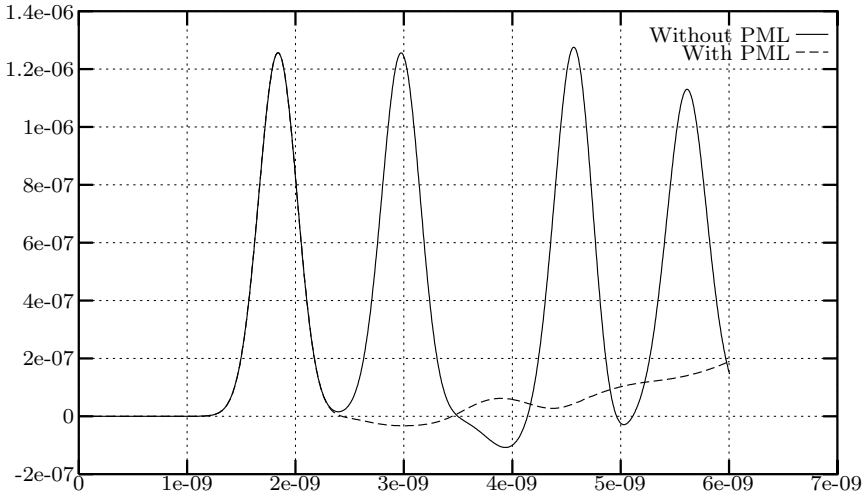

Figure 18. Observed magnetic field with and without PML on the skew grid in Figure 17. Note the increase in relative size of the reflections from Figure 16.

differencing scheme. Examples demonstrate the effectiveness of the method on Cartesian and rotated Cartesian grids in which the metric of the underlying coordinates in space is constant. As expected, the implementation is less effective on a cylindrical problem when the metric of the underlying coordinate system is not constant and the chosen form of the PML tensor is known to only produce a quasi-PML. Furthermore, the dependence of this PML on orthogonality of the coordinates is illustrated by its degradation on a skew grid problem.

ACKNOWLEGMENT

The author would first like to thank Dr. Teixeira for the opportunity to participate in this special issue and my associates Dr. Hyman and Dr. Shashkov at the Mathematical Modeling and Analysis Group at LANL for their assistance with the mimetic difference part of the project. The anonymous reviewers of the article also provided key insights into the PML formulation on the cylindrical grid and made other valuable suggestions which improved this paper. This work was supported by the Department of Energy, under contract W-7405-ENG-36.

REFERENCES

1. Balanis, C. A., *Advanced Engineering Electromagnetics,* John Wiley & Sons, New York, 1989.
2. Berenger, J.-P., "A perfectly matched layer for the absorption of electromagnetic waves," *Journal of Computational Physics,* Vol. 114, 185–200, October 1994.
3. Gedney, S. D., "An anisotropic perfectly matched layer-absorbing medium for the truncation of FDTD lattices," *IEEE Transactions on Antennas and Propagation,* Vol. 44, No. 12, 1630–1639, December 1996.
4. Gedney, S. D., "An anisotropic PML absorbing media for the FDTD simulation of fields in lossy and dispersive media," *Electromagnetics,* Vol. 16, 399–415, 1996.
5. He, J.-Q. and Q. H. Liu, "A nonuniform cylindrical FDTD algorithm with improved PML and quasi-PML absorbing boundary conditions," *IEEE Transactions on Geoscience and Remote Sensing,* Vol. 37, No. 2, 1066–1072, March 1999.
6. Hyman, J., M. Shashkov, and S. Stienberg, "The numerical solution of diffusion problems in strongly heterogeneous non-isotropic materials," *Journal of Compuational Physics,* Vol. 132, 130–148, 1997.
7. Hyman, J. M. and M. Shashkov, "Adjoint operators for the natural discretizations of the divergence, gradient and curl on logically rectangular grids," *Applied Numerical Mathematics,* Vol. 25, 413–442, 1997.
8. Hyman, J. M. and M. Shashkov, "Natural discretizations for the divergence, gradient and curl on logically rectangular grids," *Applied Numerical Mathematics,* Vol. 33, No. 4, 81–104, 1997.
9. Hyman, J. M. and M. Shashkov, "Mimetic discretizations for Maxwell's equations," *Journal of Compuational Physics,* Vol. 151, 881–909, 1999.
10. Jackson, J. D., *Classical Electrodynamics,* 2nd edition, John Wiley & Sons, New York, 1975.
11. Mittra, R. and Ü. Pekel, "A new look at the perfectly matched layer (PML) concept for the reflectionless absorption of electromagnetic waves," *IEEE Microwave and Guided Wave Letters,* Vol. 5, No. 3, 84–86, March 1995.
12. Sacks, Z. S., D. M. Kingsland, R. Lee, and J.-F. Lee, "A perfectly matched anisotropic absorber for use as an absorbing boundary condition," *IEEE Transactions on Antennas and Propagation,*

Vol. 43, No. 12, 1460–1463, December 1995.

13. Taflove, A. (ed.), *Advances in Computational Electrodynamics. The finite-difference time-domain method,* Artech House, Boston, Mass., 1998.
14. Teixeira, F. L. and W. C. Chew, "Systematic derivation of anisotropic PML absorbing media in cylindrical and spherical coordinates," *IEEE Microwave and Guided Wave Letters,* Vol. 7, No. 11, 371–373, November 1997.
15. Teixeira, F. L. and W. C. Chew, "A general approach to extend Berenger's absorbing boundary condition to anisotropic and dispersive media," *IEEE Transactions on Antennas and Propagation,* Vol. 46, No. 9, 1386–1387, September 1998.
16. Teixeira, F. L. and W. C. Chew, "PML-FDTD in cylindrical and spherical grids," *IEEE Microwave and Guided Wave Letters,* Vol. 7, No. 9, 285–287, September 1997.
17. Tong, M.-S., Y. Chen, M. Kuzuoglu, and R. Mittra, "A new anisotropic perfectly matched layer medium for mesh truncation in finite difference time domain analysis," *Int. J. Electronics,* Vol. 86, No. 9, 1085–1091, 1999.
18. Yang, B. and P. G. Petropoulos, "Plane-wave analysis and comparison of split-field, biaxial and uniaxial PML methods as ABC's for pseudospectral electromagnetic wave simulations in curvilinear coordinates," *Journal of Computational Physics,* Vol. 146, 747–774, 1998.
19. Yee, K. S., "Numerical solution of initial boundary value problems involving Maxwell's equations in isotropic media," *IEEE Transactions on Antennas and Propagation,* Vol. 14, 302–307, 1966.